Irreversibility Analysis of a Radiated Oldroyd-B Hybrid Nanofluid with Viscous Dissipation Effects

Akhtar Ali[a], Manzoor Ishaq[a] , Sami Ullah Khan[b*]

[a] *Department of Mathematics, Government College University, Faisalabad 38000, Pakistan*

[b,*] *Department of Mathematics, Namal University, Mianwali 42250,Pakistan*[*]

[*] *Corresponding author; E-mail: sk_iiu@yahoo.com*

Submitted 13/02/2026

Accepted 18/04/2026

Published 20/07/2026

DOI: 10.64518/uohjs.2026.02

Abstract:

Motivated by the enhanced thermal characteristics of hybrid nanomaterials, this study investigates heat and mass transfer in an Oldroyd-B hybrid nanofluid and assesses entropy generation. The hybrid nanofluid consists of gold (Au) and copper (Cu) nanoparticles suspended in water (H2O). A refined Fourier's thermal model is used to analyze the heat and mass transfer dynamic. The study also involves shape features, heat source, viscous dissipation and thermal radiation effects. The mass transfer is analyzed by accounting the chemical reactive species. The solution methodology is based on implementation of shooting numerical scheme. The study reveals that heat transfer enhances due to Deborah number with retardation time parameter. The entropy generation increase due to Hartmann number while declining behavior is observed for Prandtl number. Moreover, the Bejan number enhances by increasing the Eckert number. The proposed model justifies significance in thermal management systems, heat transfer optimization, control of heat dissipation in engineering systems, oil recovery, nuclear systems etc.

*Keywords**:** Entropy generation, Oldroyd-B fluid, Heat and mass transfer analysis, Shape factor, Shooting approach, Cattaneo-Christov Modelling.*

---

1. INTRODUCTION

In recent years, the topic of nanofluids is well established in industrial and engineering sectors due to its ability to improve the thermal conductivity and energy absorption. Nanofluids are formed by dispersing nanosized (1-100 nm) particles into base fluid as like water, ethylene glycol, oil and engine oil. The sustainability and compatibility of traditional fluid improved by adding nanoparticles. Solar thermal collectors are very incredible application of nanofluid, nanofluids empower the thermal efficiency of solar system to enhance the absorbing ability of sunlight to increase the heat transfer process. Nanofluids are essential to increases the cooling and heating efficiency of thermal systems. Nanofluids facilitate rapid heat transfer, reduce energy loss, and contribute to various aspects of system sustainability. The superior heat transfer characteristics of nanofluids justify applications in various sectors, including, solar heaters, photovoltaic-thermal systems, heat exchangers, and industrial thermal management applications. Further, a suitable choice of nanoparticles boosts up the heat transfer process. Assad et al. (2021) focused on heat exchanger appliations by adding nanoparticles in base fluids within different flow constraints. Kumar et al. (2021) reviewed the methods of preparation of nanofluids used in recent years for heat transformation in heat exchangers. Ali et al. (2021) investigated the development of nanofluids for enhancing heat transfer processes in various industries, specifically focusing on carbon particles suspended in a base fluid. Pavía et al. (2021) observed the improvement of thermal conductivity of base fluid with the suspension of graphene nanoparticles. Sharma et al. (2022) explored the advancement of nanofluids in renewable energy systems with implementation of a machine learning approach. The advancement in the sector of oil refinery by using nanofluids on behalf of various kinds of nanoparticles was found by Khoramian et al. (2022). The thermal insights of magneto-radiative Williamson nanofluid model within various flow constraints across stretchable porous sheet was examined by Abbas et al. (2022). The synthesis, preparation approach and applications of nanofluids in various industrial and engineering sectors were syncretised by Wang et al. (2023). Bhatti et al. (2022) studied the novality of nanofluids with various nanoparticles immersed in base fluid across renewable energy field. Nabwey et al. (2022) deliberated the role of nanofluids in heat transmission mechanism across porous medium. The numerical computation of magnetised Maxwell nanofluid by adding non-Linear thermal radiative impact via activation energy were described by Ahmed et al. (2024). Bani-Fwaz et al. (2024) computed the thermal enhancement of magnetised radiative nanofluid flow with the suspension of aluminium oxide in water as a base fluid. The heat transformation via Carreau–Yasuda nanofluid model in case of variable thermal conductivity and quadratic convection were performed by Akbar et al. (2024). Sohail et al. (2025) explored magneto-radiative Maxwell fluid in the presence of Bio-Convective boundary constraints across stretchable porous sheet by implementation of HAM solution. In order to perform a more thorough thermal analysis, Ahmad et al. (2025) used the Cattaneo–Christov heat flux framework and an external heat source to study buoyancy-driven bidirectional forced convection in a chemically reactive Oldroyd-B nanofluid. Shoaib et al. (2023) performed the stochastic numerical simulatons for studying thermal behavior of Carreau nanofluid. Aamir et al. (2025) addressed the computing analysis for visualzing thermal reflection of micropolar nanofluid.

Hybrid nanofluids emerged as one of the most promising advancements in thermal engineering across its thermal characteristics. Hybrid nanofluids has become a central focus of research for many researchers and industrialists due to its more quickly heat transfer process ability. The consists of two types of nanoparticles makes hybrid nanofluid that improves the thermal conductivity and rate of heat transparency. The absorbing and energy-losing capability of hybrid nanofluids makes them more attractive in the sector of solar collector systems, still in the presence of variability of sunlight constraints. The thermal enhancing characteristics of hybrid nanofluids make m more effective in various sectors including, flat plate collectors, PV/T systems, parabolic trough collectors. Further, the applications of hybrid nanofluids in thermal systems are very advantageous for industrialists. Such as reduced thermal resistance, better cooling and heating efficiency in heat exchangers make more superior thermal management system. The combined impacts of nanoparticles that ensure high stability operation, grooming energy and less operational costs. The thermal conductance and heat generative impacts on magnetised hybrid nanofluid in the presence of slip conditions immersed in porous media was assessed by Eid et al. (2022). The rheological nature of hybrid nanofluid in industrial sector were presented by Esfe et al. (2022). Asghar et al. (2023) fluctuated magnetized mixed convective hybrid nanofluid with heat generative/absorptive impacts across velocity slip constraints. Shah et al. (2023) employed the Cattaneo–Christov model to numerically investigate Prandtl–Eyring hybrid nanofluid flow based on radiative engine oil. Mebarek-Oudina et al. (2024) analysed the thermal performance of MHD hybridised-nanofluid with convection and porous media corporation across entropy generation. Cu–CuO hybrid nanofluid flows over a convectively heated surface were numerically compared by Algehyne et al. (2024) using water and kerosene oil. Viscosity dissipation effects in unsteady MHD Casson hybrid nanofluid flow across a stretching surface were studied by Rehman et al. (2024). The machine learning-based thermal performance of hybrid nanofluid flow across a stretched sheet was focused by Khan et al. (2023).

The Oldroyd-B fluids are classified as rate-type fluids that exhibit viscoelastic properties, reflecting the characteristics of complex fluids that possess both elasticity and viscosity. The deforming ability of this fluid deliberates the flow behaviour of polymer solutions and dilute polymeric liquids. The Oldroyd-B fluids model enriches many applications in biomedical fields where viscoelastic property exists. Also, to analysis the blood behaviour via this model provides better outcomes. Further, this model plays an important role in the microfluidic systems to estimates the flow stability and outcomes in case of numerous shear constraints. However, the Oldroyd-B model is widely used in chemical and industrial process to enhance mixing, coating, and extrusion operations within non-Newtonian fluids. The hydro-thermo-fluidic behavior of an Oldroyd-B hybrid nanofluid at low and moderate Prandtl numbers was investigated by Gope et al. (2023). Absorbing boundary conditions for magnetized Oldroyd-B fluid flow over a semi-infinite plate were developed by Liu et al. (2024). Munir et al. (2025) fluctuated the entropy generation by using Oldroyd-B nanofluid model via computing analysis. Heat transfer in bioconvective Oldroyd-B nanofluids with nonlinear radiation and activation energy was modeled by Razzaq et al. (2025) using artificial neural networks.

1.1. Objectives of present work

This investigation presents the heat and mass transfer due to Oldroyd-B hybrid nanofluid with applications of entropy generation. The HNF features are observed with uniform suspension of gold (Au)and copper (Cu)) nanoparticles in water (H_2O) base fluid. The choice of Au and Cu is associated to enhanced thermal features and stable conducting consequences. The heat-transfer characteristics are examined using the Cattaneo-Christov model, with viscous dissipation and radiation effects included. The shape features effects are further attributed to analyze the thermal transport. Mass transfer investigation is assessed through chemical reaction consequences. A dimensionless system is obtained for modeled problem which is further numerically compiled. Physical dynamic of problem is addressed for mono and hybrid nanofluids.

1.2. Novelty of the current research

The proposed mathematical model endorsed thermal reflection of Oldroyd-B HNF $(Au - Cu)/H_2O$ with applications of shape features and entropy generation. The investigation of heat and mass transfer with entropy generation assessment is important to optimize the thermal performance of transport system. The understanding of shape features determined the thermal performance of hybrid nanoparticles. The novelty of current model further lies in assessment of Bejan number, influencing the irreversibility process in thermal transport systems. The model may be justifying applications in advanced engineering applications, energy systems, thermal management devices and industrial heat exchangers (Aziz et al. (2025)).

2. Mathematical formulation

A two-dimensional flow of Oldroyd-B hybrid nanofluid is considered over elastic surface. A colloidal suspension of two types of nanomaterials such as copper(Cu) and gold(Au) within water (H_2O)as a base fluid entertains hybrid nanofluid. The velocity of surface is defined by $u_w = ax$, where a is the stretched constant. To employ the magnetic field perpendicular to the sheet. The horizontal and vertical component of velocity within x and $y$axis evaluates with $u and v$ as predicted via Fig. 1. The implementation of magnetic field B_0 is perpendicular to sheet, where B_0 shows their magnitudes. The innovation of the current work arises from the analysis of entropy generation using the Bejan number. Governing equations are:

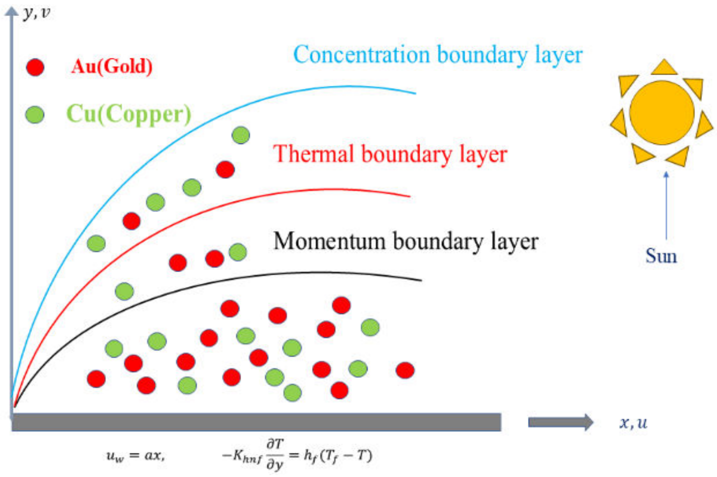

Fig. 1: Flow geometry.

$$\frac{\partial u}{\partial x} + \frac{\partial v}{\partial y} = 0, \tag{1}$$

$$u\frac{\partial u}{\partial x} + v\frac{\partial u}{\partial y} + \varepsilon_0\left(u^2\frac{\partial^2 u}{\partial x^2} + v^2\frac{\partial^2 u}{\partial y^2} + 2uv\frac{\partial^2 u}{\partial x \partial y}\right) = \nu_{hnf}\frac{\partial^2 u}{\partial y^2} + \varepsilon_1\nu_{hnf}\left[u\frac{\partial^3 u}{\partial x \partial y^2} - \frac{\partial u}{\partial x}\frac{\partial^2 u}{\partial y^2} - \frac{\partial u}{\partial y}\frac{\partial^2 v}{\partial y^2} + v\frac{\partial^3 u}{\partial y^3}\right] - \frac{\sigma_{hnf}{B_0}^2}{\rho_{hnf}}\left(u + \varepsilon_0 v\frac{\partial u}{\partial y}\right), \tag{2}$$

$$u\frac{\partial T}{\partial x}+v\frac{\partial T}{\partial y}+\varepsilon_2\begin{bmatrix}u\frac{\partial v}{\partial x}\frac{\partial T}{\partial y}+u^2\frac{\partial^2 T}{\partial x^2}+v^2\frac{\partial^2 T}{\partial y^2}\\+2uv\frac{\partial^2 T}{\partial x\partial y}+v\frac{\partial u}{\partial y}\frac{\partial T}{\partial x}+v\frac{\partial v}{\partial y}\frac{\partial T}{\partial y}\\+u\frac{\partial u}{\partial x}\frac{\partial T}{\partial x}\end{bmatrix}=\frac{1}{(\rho C_p)_{hnf}}\begin{bmatrix}\left(K_{hnf}+\frac{16\Omega T_\infty^{\ 3}}{3k^*}\right)\frac{\partial^2 T}{\partial y^2}+\mu_{hnf}\frac{\varepsilon_1}{\varepsilon_0}\left(\frac{\partial u}{\partial y}\right)^2\\+\sigma_{hnf}B_0^{\ 2}u^2+Q(T-T_\infty)\end{bmatrix}\quad(3)$$

$$u\frac{\partial C}{\partial x}+v\frac{\partial C}{\partial y}+\varepsilon_3\begin{bmatrix}v\frac{\partial u}{\partial y}\frac{\partial C}{\partial x}+v\frac{\partial v}{\partial y}\frac{\partial C}{\partial y}+u\frac{\partial v}{\partial x}\frac{\partial C}{\partial y}\\+2uv\frac{\partial^2 C}{\partial x\partial y}+u^2\frac{\partial^2 C}{\partial x^2}+v^2\frac{\partial^2 C}{\partial y^2}\\+u\frac{\partial u}{\partial x}\frac{\partial C}{\partial x}\end{bmatrix}=D_B\frac{\partial^2 C}{\partial y^2}-k_r(C-C_\infty).\quad(4)$$

In above formulated problem, ρ_{hnf} presents the density of hybrid nanofluid, μ_{hnf} is the dynamic viscosity, B_0 predicts intensity of magnetic influence, σ_{hnf} is electrical conductivity, Ω is the Stefan Boltzmann coefficient, K_{hnf} indicates thermal conduction, $(\rho C_p)_{hnf}$ describe specific heat capacity of hybrid nanofluid, D_B exhibits Brownian motion diffusivity, k_r shows chemical reactivity, ε_2 demonstration of concentration relaxation parameter, ε_0 denotes relaxation constant, ε_1 , ε_3 portrayed concentration constant.

Thermal boundary constraints with convective characteristics:

$$\left.\begin{aligned}&u=u_\omega=ax, C=C_w, v=0, -k_{hnf}\frac{\partial T}{\partial y}=h_f(T_f-T), at y=0,\\&u\to 0,\frac{\partial u}{\partial y}\to 0,\frac{\partial^2 u}{\partial y^2}\to 0, T\to T_\infty, C\to C_\infty, y\to\infty.\end{aligned}\right\}\quad(5)$$

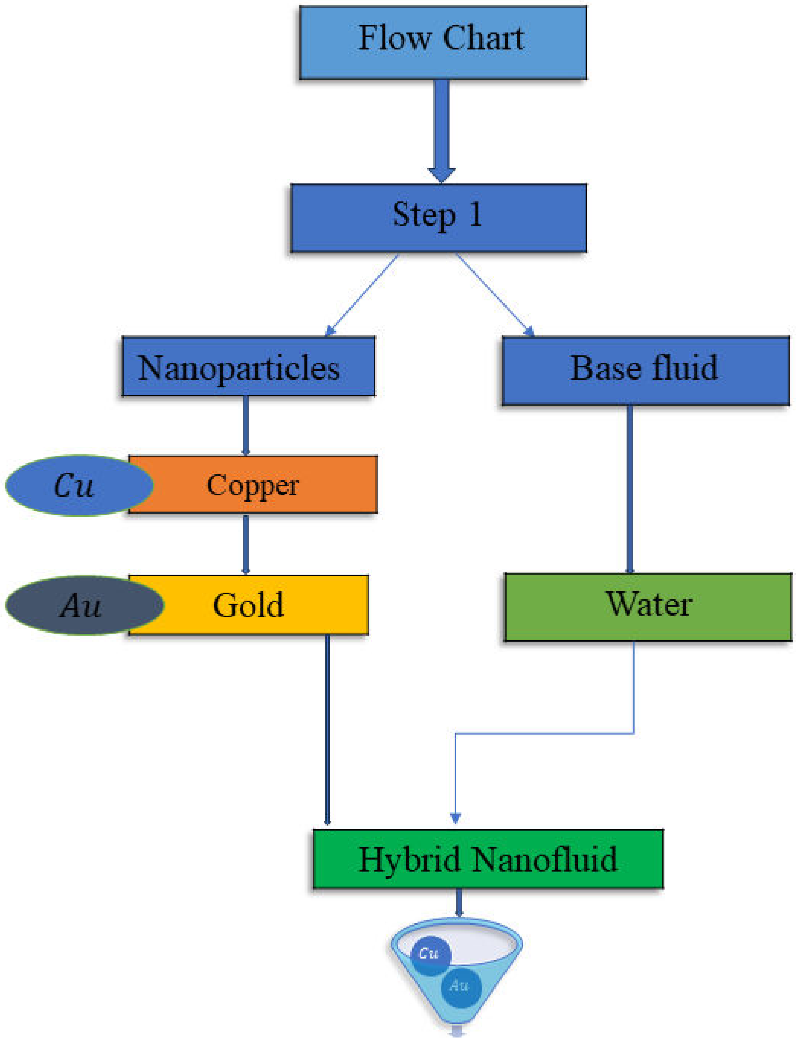

Fig. 2: Encapsulated suspension process of nanomaterials into base fluid.

2.1 Appropriate similarity technique

Similarity transformations are (Khan et al. (2025)).

$$v = -\sqrt{\nu_f a} f, \theta = \frac{T - T_\infty}{T_w - T_\infty}, \eta = \sqrt{\frac{a}{\nu_f}} y, u = axf', \phi = \frac{C - C_\infty}{C_w - C_\infty}. \quad (6)$$

Simplification

$$A_1\left[f''' - \beta_2\left(ff^{iv} - f''^2\right)\right] - A_3 M\left(\beta_1 ff'' - f'\right) + A_2\left[-f'^2 + ff'' + \beta_1\left(2ff'f'' - f^2 f'''\right)\right] = 0, \quad (7)$$

$$(A_4 + R)\theta'' + Pr\left[A_1 \frac{\beta_2}{\beta_1} Ecf''^2 + A_3 MEcf'^2 + \chi\theta\right] - A_5 Pr\left[\beta_3\left(f^2\theta'' + ff'\theta'\right) - f\theta'\right] = 0, \quad (8)$$

$$\phi'' + Sc\left[\left(\beta\phi + f\phi'\right) - \delta_C\left(ff'\phi' + f^2\phi''\right)\right] = 0. \quad (9)$$

The results of thermal boundary constraints as below

$$\left.\begin{array}{l} f(0) = 0, \phi(0) = 1, A_4\theta'(0) = -Bi[1 - \theta(0)], f'(0) = 1 \, at \, \eta = 0, \\ f'(\infty) \to 0, f''(\infty) \to 0, \theta(\infty) \to 0, \phi(\infty) \to 0 \, at \, \eta \to \infty. \end{array}\right\} \quad (10)$$

Where $M = B_0^2 \sigma_f / a \rho_f$ is the magnetic parameter, $\beta_1 = \varepsilon_0 a$ is the Maxwell relaxation time parameter, $\beta_2 = \varepsilon_1 a$ illustrates the momentum retardation dimensionless number, $Pr = \upsilon_f\left(\rho C_p\right)_f / k_f$ be Prandtl number, $Ec = U_w^2 / C_p(T_w - T_\infty)$ is Eckert parameter, $\beta_3 = a\varepsilon_2$ describe thermal relaxation parameter, $\beta = Kr/a$ demonstrates chemical reactive number, $Sc = \nu_f / D_B$ shows Schmidt number, $\delta_C = \varepsilon_3 a$ be thermal concentration, $R = 16\Omega T_\infty^3 / 3kk^*$ evaluates the thermal radiation number , $\lambda = Q_0 / \left(\rho C_p\right)_f a$, aligned external heat source number, $Bi = h_f / k_f \sqrt{\upsilon_f / a}$ outlined Biot number.

Some thermal constants are

$$A_1 = \frac{\mu_{hnf}}{\mu_{nf}}, A_2 = \frac{\rho_{hnf}}{\rho_{nf}}, A_3 = \frac{\sigma_{hnf}}{\sigma_{nf}}, A_4 = \frac{K_{hnf}}{K_{nf}}, A_5 = \frac{(\rho C_p)_{hnf}}{(\rho C_p)_{nf}}.$$

Table 1: The significance of nanomaterials with geometrical emergence (Khan et al. (2025)).

Geometrical appearance			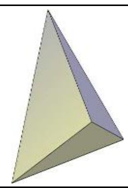		
Z Shape	3.0 Sphere	3.7321 Hexahedron	4.0613 Tetrahedron	4.9 Cylinder	6.3678 Column

Table 2: Enclosed the thermophysical properties of gold (Au) and copper(Cu) nanoparticles within water(H_2O) as a base fluid /

Physical Properties	Au 	Cu 	(H_2O) 
$\rho(kgm^{-3})$	8933	5180	997.1
$C_p(Jkg.k)$	385	670	4179
$\kappa(W.(m.k))$	401	9.7	0.613

Table 3: Comparison of Hybrid and Mono nanofluid properties

Characteristics	Nanofluid and Hybrid Nanofluid
Density $\rho(kgm^{-3})$	$\rho_{nf} = (1-\phi_1)\rho_f + \phi_1\rho_{r1}$ $\rho_{hnf} = (1-\phi_2)[(1-\phi_1)\rho_f + \phi_1\rho_{r1}] + \phi_2\rho_{r2}$
Heat Capacity $C_p(Jkg.k)$	$(\rho C_p)_{nf} = (1-\phi_1)(\rho C_p)_f + \phi_1(\rho C_p)_{r1}$ $(\rho C_p)_{nf} = (1-\phi_2)\left[(1-\phi_1)(\rho C_p)_f + \phi_1(\rho C_p)_{r1}\right] + \phi_2(\rho C_p)_{r2}$
Dynamic Viscosity $\mu(Pa.s)$	$\mu_{nf} = \frac{\mu_f}{(1-\varphi_1)^{2.5}}$ $\mu_{nf} = \frac{\mu_f}{(1-\varphi_1)^{2.5}(1-\varphi_2)^{2.5}}$
Electrical conductivity $\sigma(S.m^{-1})$	$\sigma_{nf} = 1 + \frac{3\left(\frac{\sigma_{r1}}{\sigma_f}-1\right)\phi_1}{2+\frac{\sigma_{r1}}{\sigma_f}-\left(\frac{\sigma_{r1}}{\sigma_f}-1\right)\phi_1} * \sigma_f$ $\sigma_{hnf} = \frac{\sigma_{r1} + (S_f-1)\sigma_{nf} - (S_f-1)\phi_2(\sigma_{nf}-\sigma_{r2})}{\sigma_{r2} + (S_f-1)\sigma_{nf} - \phi_2(\sigma_{nf}-\sigma_{r2})} * \sigma_{nf}$
Thermal Conductivity $\kappa(W.(m.k))$	$k_{nf} = \frac{k_{r1} + (s_f-1)k_f - (s_f-1)\phi_1(k_f-k_{r1})}{k_{r1} + (s_f-1)k_f + \phi_1(k_f-k_{r1})} * k_f$ $k_{nf} = \frac{k_{r2} + (s_f-1)k_{nf} - (s_f-1)\phi_2(k_{nf}-k_{r2})}{k_{r2} + (s_f-1)k_{nf} + \phi_2(k_{nf}-k_{r2})} * k_{nf}$

2.2. Engineering Quantities

The skin friction $Re_x^{\frac{-1}{2}}\,C\,f_x$, Nusselt number $\left(Re_x^{\frac{-1}{2}}\,N\,u_x\right)$ and Sherwood number $\left(Re_x^{\frac{-1}{2}}\,S\,h_x\right)$ plays an important role in engineering sector. The skin friction coefficient calculates the friction forces that faces the fluids flow across the surface. The heat generation and mass dissipation estimation is manifested via Nusselt and Sherwood number. The mathematical formulation of above engineering entities is elucidated below via equation (11)

$$C_f = \frac{\tau_w}{\rho_f U_w{}^2}, Nu_x = \frac{q_w x}{k_f(T_w - T_\infty)}, Sh_x = \frac{x j_s}{D_B(C_w - C_\infty)}.$$

$$\tau_w = \mu_{hnf}\left(\frac{\partial u}{\partial y}\right)_{y=0}, q_w = -k_{hnf}\left(1 + \frac{16}{3}\frac{\sigma^* T_\infty{}^3}{k^* k_{hnf}}\right)\left(\frac{\partial T}{\partial y}\right)_{y=0}, j_s = -D_B\left(\frac{\partial C}{\partial y}\right)_{y=0}. \quad (11)$$

After evaluation with equation (11)

$$\left.\begin{aligned} &\frac{1}{2}C_f\,\mathrm{Re}_x{}^{1/2} = A_1 f''(0), \\ &Nu_x\,\mathrm{Re}_x{}^{-1/2} = -(A_4 + R)\theta'(0), \\ &\mathrm{Re}_x{}^{1/2}\,Sh_x = -\phi'(0). \end{aligned}\right\} \quad (12)$$

3. Solution methodology

A standard shooting method is employed to perform the numerical simulations. The choice of shooting technique is based on best convergence. A step size of $\Delta\eta = 0.02$ is used for simulations. The accuracy of the solution is maintained up to 10^{-4}. For changing the problem into a first-order system, the following variables are introduced:

$$f = y_1, f' = y_2, f'' = y_3, f''' = y_4, f^{iv} = y_4{}',$$
$$\theta = y_5, \theta' = y_6, \theta'' = y_6{}',$$
$$\phi = y_7, \phi' = y_8, \phi'' = y_8{}'. \quad (13)$$

Resulting

$$y_4{}' = \frac{1}{\beta_2 A_1 y_1}\left[A_1(y_4 + \beta_2 y_3{}^2) + A_3 M(y_2 - \beta_1 y_1 y_3) - A_2[y_2{}^2 - y_1 y_3{}^2 + \beta_1 y_1{}^2 y_4 - 2y_1 y_2 y_3]\right], (14)$$

$$y_6{}' = \frac{-Pr\left[A_1 \frac{\beta_2}{\beta_1} Ec y_3{}^2 + A_3 M Ec y_2{}^2 + \lambda y_5\right] + A_5 Pr[\beta_3 y_1 y_2 y_6 - y_1 y_6]}{[(A_4 + R) - A_5 Pr \beta_3 y_1{}^2]}, \quad (15)$$

$$y_8{}' = \frac{Sc[y_8 y_1 - \delta_c y_1 y_2 y_8 + \beta y_7]}{1 - \delta_c y_1{}^2}. \quad (16)$$

$$\left.\begin{array}{l} y_1(0) = 0, y_2(0) = 1, A_4 y_6(0) = -Bi[1 - y_5(0)], y_7(0) = 1, at\eta = 0, \\ y_2(\infty) \to 0, y_3(\infty) \to 0, y_5(\infty) \to 0, y_7(\infty) \to 0, at\eta \to \infty. \end{array}\right\} \quad (17)$$

4. Entropy Generation

Entropy generation for the present problem is expressed as follows.

$$E_G = \underbrace{\frac{k_{hnf}}{T^2}\left(\frac{\partial T}{\partial y}\right)^2}_{heattransferIrreversibility} + \underbrace{\frac{\sigma_{hnf} B_0{}^2 u^2}{T}}_{JouleheatIrreversibility} + \underbrace{\frac{\mu_{hnf}}{T}\frac{\varepsilon_1}{\varepsilon_0}\left(\frac{\partial u}{\partial y}\right)^2}_{fluidfrictionIrreversibility} + \underbrace{\frac{Q(T - T_\infty)}{T}}_{heatsourceIrreversibility} \quad (18)$$

The rate of entropy production across dimensionless variables elucidates as below

$$N_s = \frac{E_G}{(E_G)_0} = A_5 \frac{\theta'^2}{(\theta + \varpi)^2} + Pr\left(A_2 \frac{\beta_2}{\beta_1} \frac{Ecf'^2}{(\theta + \varpi)} + A_3 \frac{Ecf'^2 M}{(\theta + \varpi)} + \frac{\lambda\theta}{(\theta + \varpi)}\right), (19)$$

The dimensionless temperature gradient has been predicted by $(E_G)_o = \frac{k_f a}{\nu_f} and \varpi = \frac{T_\infty}{T_w - T_\infty}$.

The mathematical formulation of Bejan number has been explored via equation (20)

$$Be = \frac{A_5 \frac{(\theta')^2}{(\theta + \varpi)^2}}{A_5 \frac{(\theta')^2}{(\theta + \varpi)^2} + Pr\left(A_2 \frac{\beta_2 Ecf''^2}{\beta_1(\theta + \varpi)} + A_3 \frac{EcMf'^2}{(\theta + \varpi)} + \frac{\lambda\theta}{(\theta + \varpi)}\right)}. \quad (20)$$

$$Be = \begin{cases} 0 totalirreversibilitiesdo\min a tesheattransfer \\ \frac{1}{2} totalirreversibilitiesequaltoheattransferirreversibility \\ 1 heatflowirreversibilitydo\min a tes \end{cases} \quad (21)$$

5. Graphical Analysis

This section leads to physical understating of problem subject to diverse variation of parameters like Hartmann number(M), relaxation parameter (β_1) and retardation parameter (β_2), Prandtl number $(Pr())$, Eckert number(Ec), heat source number(λ), thermal relaxation number (β_3) and concentration(δ_c) parameter, chemical reactive number(β), Schmidt number(Sc) and Radiation number(R). The investigation comprises comparative analysis of results for mono nanofluid $(Au - H_2 O)$ and hybrid nanofluid $(Au - Cu - H_2 O)$. Physical significance of Hartmann parameter (M) on velocity profile f' has been visualized in Fig. 1(a). A declining trend in f' is noticed with enlarging values of M. This trend is observed due to the resistive nature of the Lorentz force. Fig. 1(b) provides undersetting of f' due to the retardation parameter β_2. It is noted that the retardation time enhances the profile of f'. The results contributed in Fig. 1(c) explore the results for f' by varying relaxation number β_1. The fluid velocity is suppressed due to β_1. The observations for f' subject to nanoparticles volume fraction ϕ_1 are exhibited in Fig. 1(d). The velocity f' declines by increasing ϕ_1.

Fig. 2(a) incorporates the thermal behavior of radiation number R on temperature profile θ. It is noticed that θ is enhanced with enlarging R. Such an improved thermal profile is associated with the transfer of energy through electromagnetic waves. Fig. 2(b) demonstrates the impact of Prandtl number Pr on θ. A declining trend in heat transfer rate is observed for higher Pr. These outcomes physically involve the low thermal diffusivity. The thermo-physical behavior of heat source number λ on θ has been investigated in Fig. 2(c). Enhancing change in θ is predicted due to λ. This enhancement in thermal behavior is subject to an additional source of energy, which increases the heat transfer impact. Fig. 2(d) illustrates the results for the significance of Eckert number Econ θ. A positive response for heat transfer occurs with the increase of Ec. Such enhancement in thermal profile is associated to kinetic energy due to viscous dissipation. The physical scenario of retardation parameter β_2 on θ is analyzed in Fig. 2(e).

Larger β_2 leads to improvement of θ. Fig. 2(f) explains the features of β_1 on θ. The profile of θ slows down due to β_1. Fig. 2(g) presents the fluctuation in θ for Biot number Bi. The heat transfer grows by increasing Bi, which is subject to direct relation of Bi with the coefficient of heat transfer. The results for shape factor coefficient on heat transfer evaluation are deduced via Fig. 2(h), providing declining thermal behavior.

The impact of Schmidt number Sc on concentration profile ϕ is simulated in Fig. 3(a). A declining growth in profile of ϕ is inspected. Such outcomes physically account the reverse relation of Schmidt number with mass diffusivity. The trend of chemical reactive number β against ϕ has been described in Fig. 3(b). Declining change in ϕ is noted upon increasing β. The influence of thermal concentration parameter δ_c on ϕ is shown in Fig. 3(c). Higher δ_c leads to decrement in ϕ.

Figure 4(a) shows the variation of the skin-friction coefficient with β_2 for different values of M. The skin friction showing a declining impact for larger β_2. The Nusselt number profile $Re_x^{\frac{-1}{2}} N u_x$ variation with R by varying β_3 and Ec are explain in Fig. 4(b). The Nusselt number enriches for both parameters. Fig. 4(c) also confirms an enhancement of $Re_x^{\frac{-1}{2}} N u_x$ by increasing β_3 and Ec.

The results for entropy generation N_s subject to variation of various parameters such as Hartmann number (M), Prandtl number(Pr), Eckert number(Ec) and heat source number(λ) are responded in Fig. Fig. 5(a-d). Fig. 5(a) fluctuates the alteration of entropy generation against Hartmann number (M). Entropy is enhanced with enlarging M.The influence of Pr on N_s is attributed in Fig. 5(b). Change in Pr declines N_s. The visualization of Eckert number on N_s are investigated in Fig. 5(c). The entropy generation is maximum due to Ec. Fig. 5(d) also possess similar observations where results for λ are proposed.

Fig. 6(a) demonstrates the impact of Hartmann number on Bejan number. The Bejan number grows against higher M. Fig. 6(b) expresses the physical significance of γ on Bejan profile. It noted that change in γ enhances the Bejan profile. The illustration of Bejan number by varying β_2 is visualized in Fig. 6(c). The Bejan number increasing due to β_2. Table 4 illustrates the numerical outcomes for skin friction coeffienct for mono and hybrid nanofluids by varying flow parameters. Table 5 shows that Nusselt number increases due to λ and β_3. Comparative numerical values demonstrate that hybrid nanofluid shows more prominent variation as compared to MNF. Table 6 encapsulates the results for Sherwood number which shows increasing trend for δ_c and Sc.

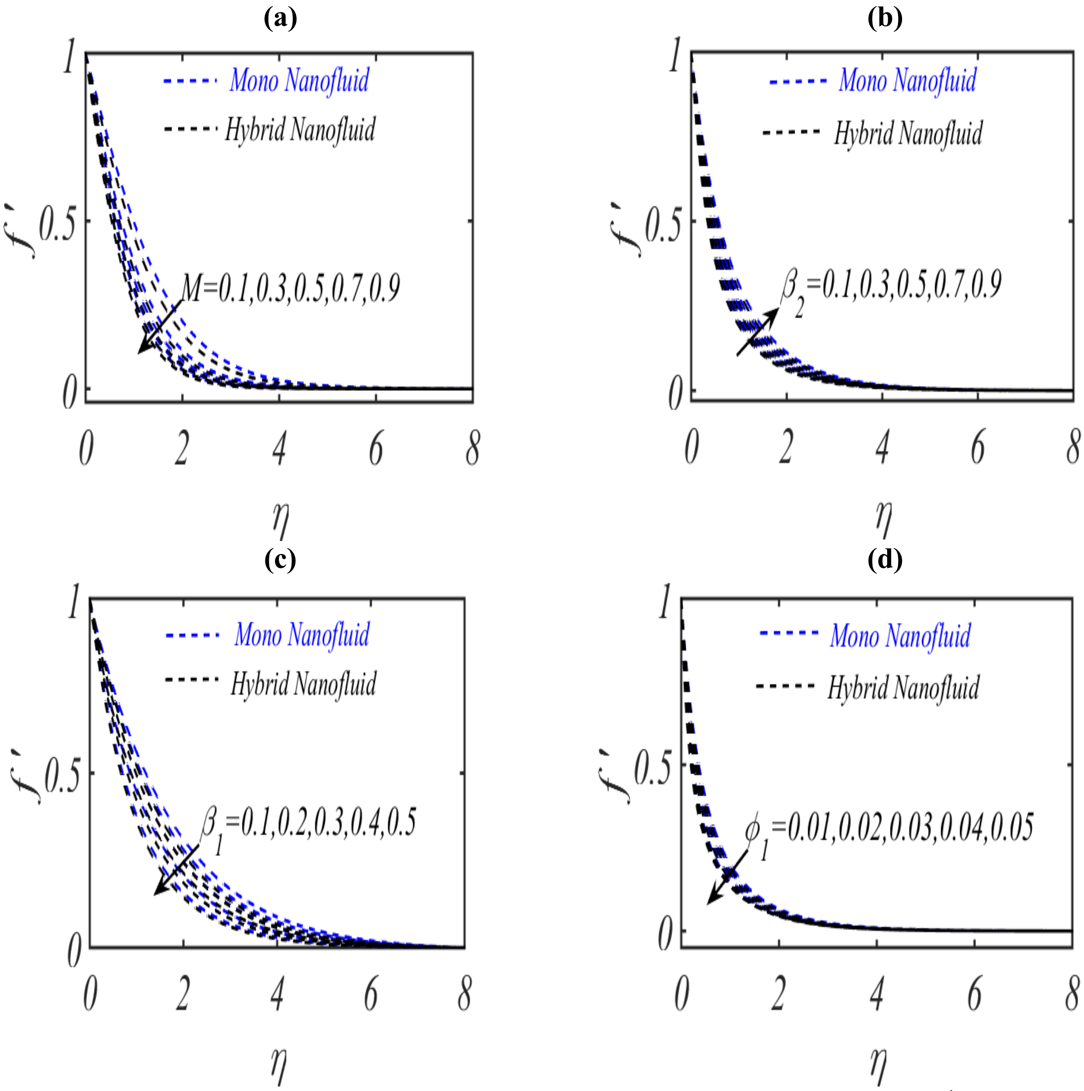

Fig. 1(a-d): Effects of (a) M (b) β_2 (c) β_1 (d) ϕ_1 on velocity profile $f^{'}$.

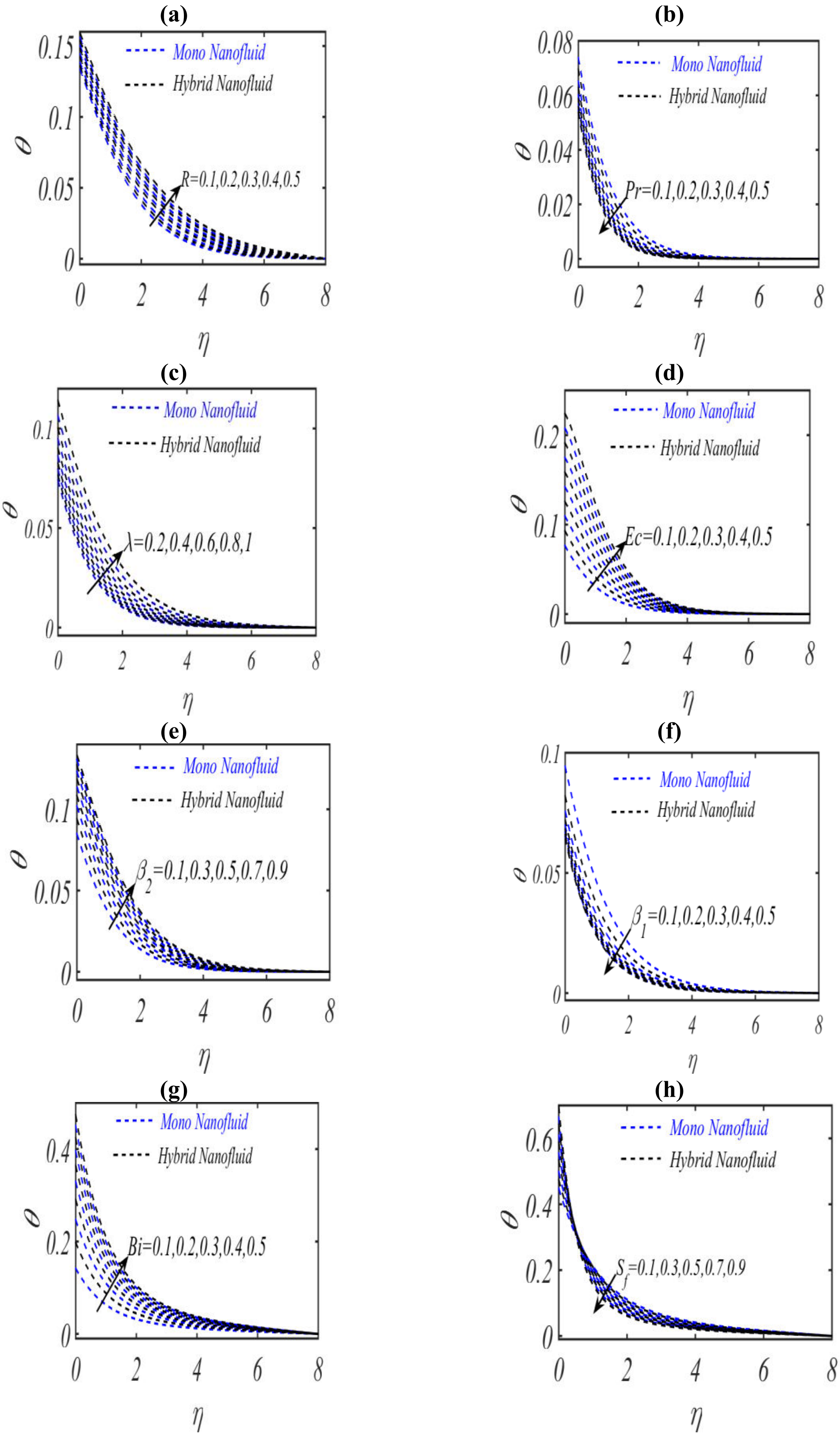

Fig. 2(a-h): Effect of (a) R (b) Pr (c) λ (d) Ec (e) β_2 (f) β_1 (g) Bi (h) S_f on temperature profile θ.

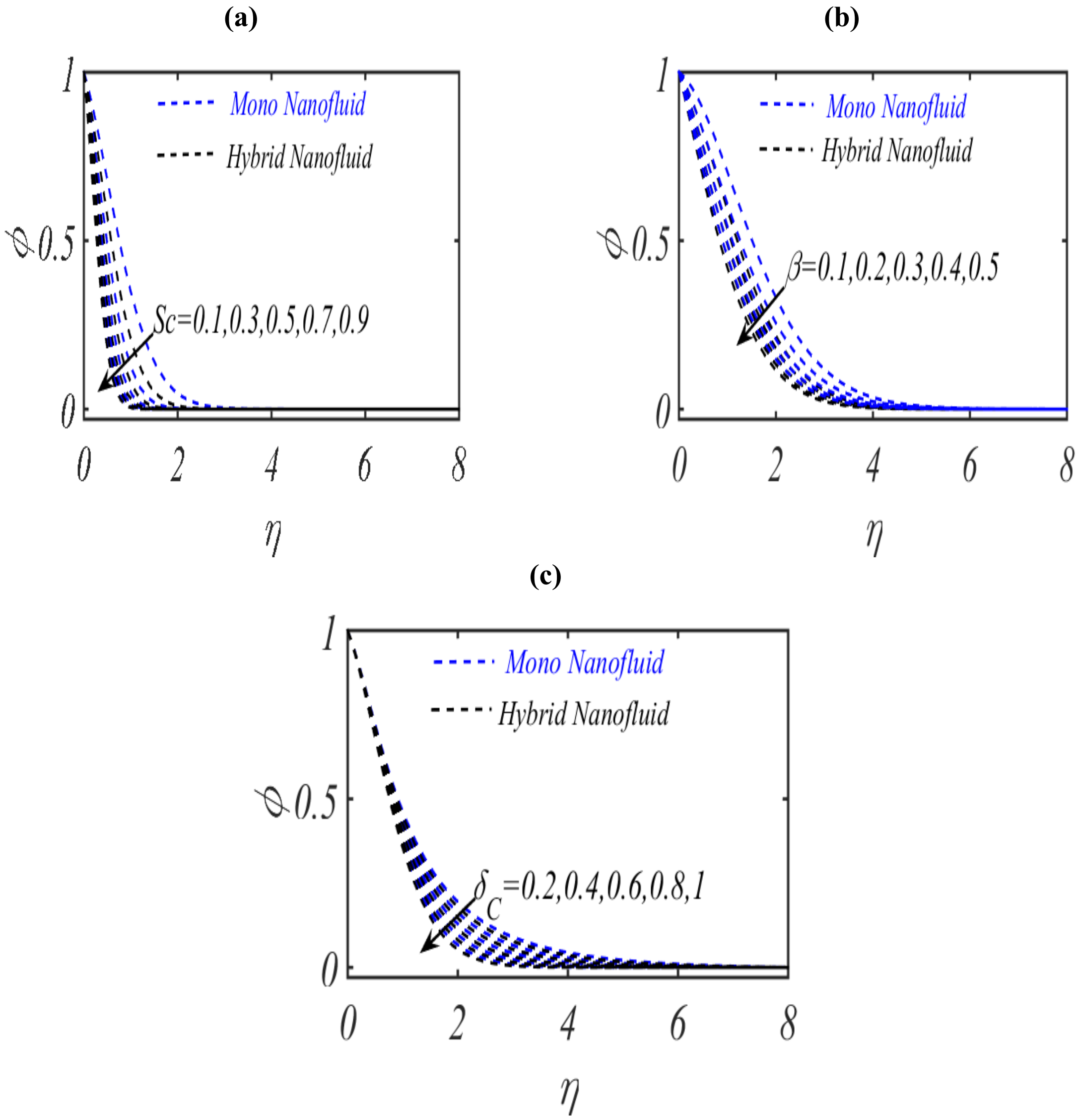

Fig. 3(a-c): Effects of (a) Sc (b) β (c) δ_c across concentration profile ϕ.

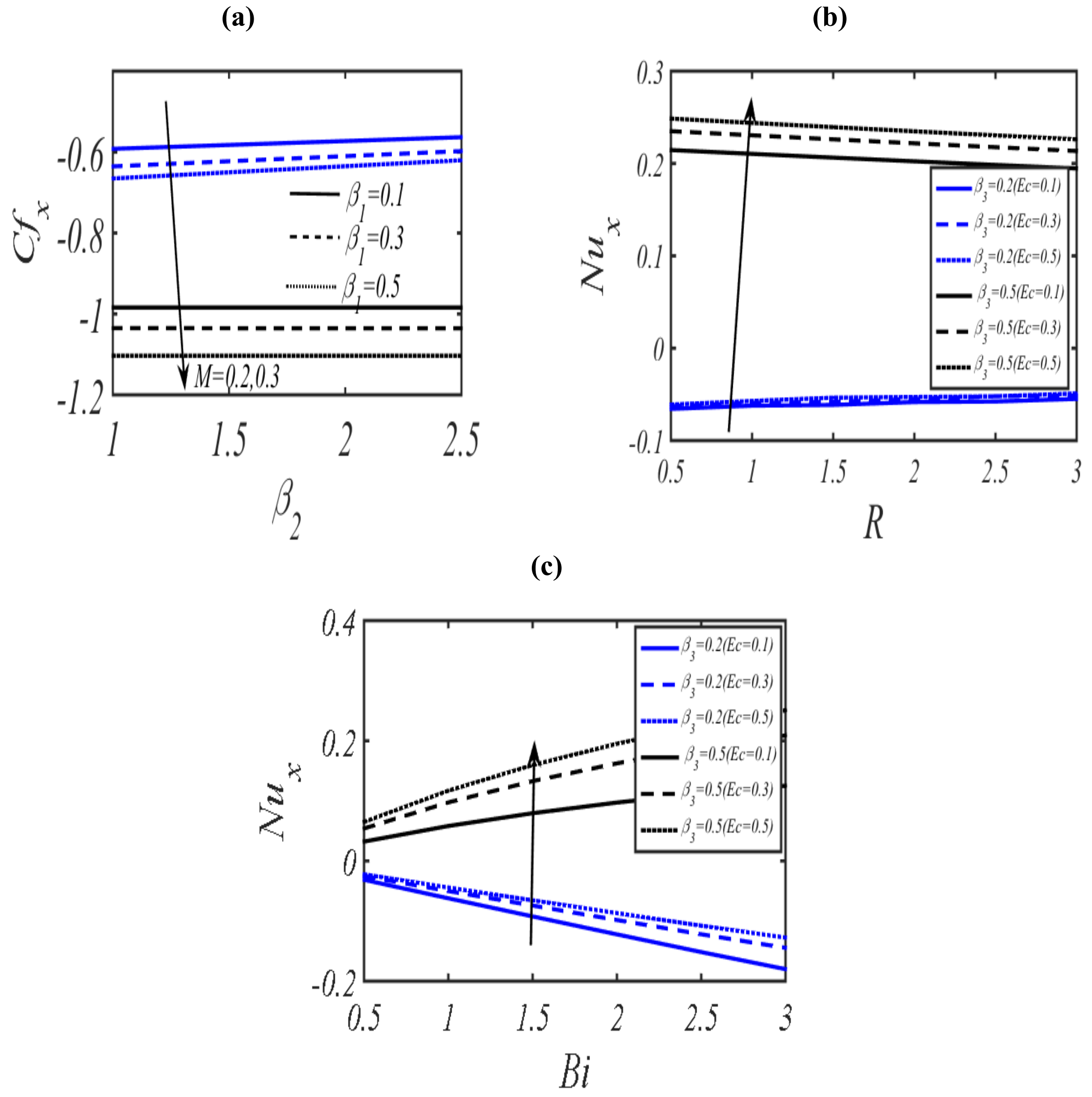

Fig. 4(a-c): Variations of skin friction and Nusselt number against (a) β_2 versus M (b) R versus Ec (c) Bi versus Ec.

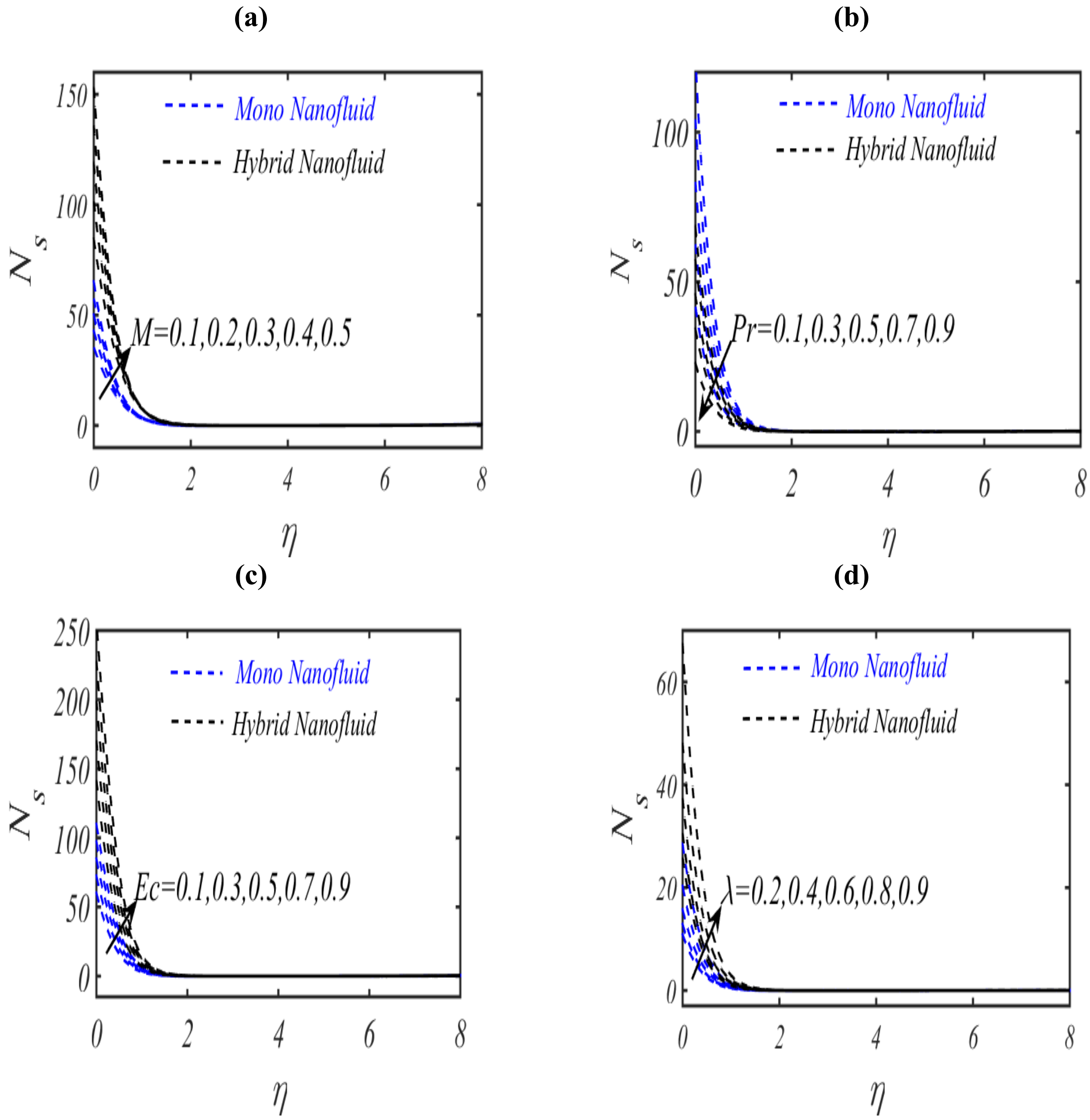

Fig. 5(a-d): Variation of entropy generation for (a) M (b) Pr (c) Ec (d) λ.

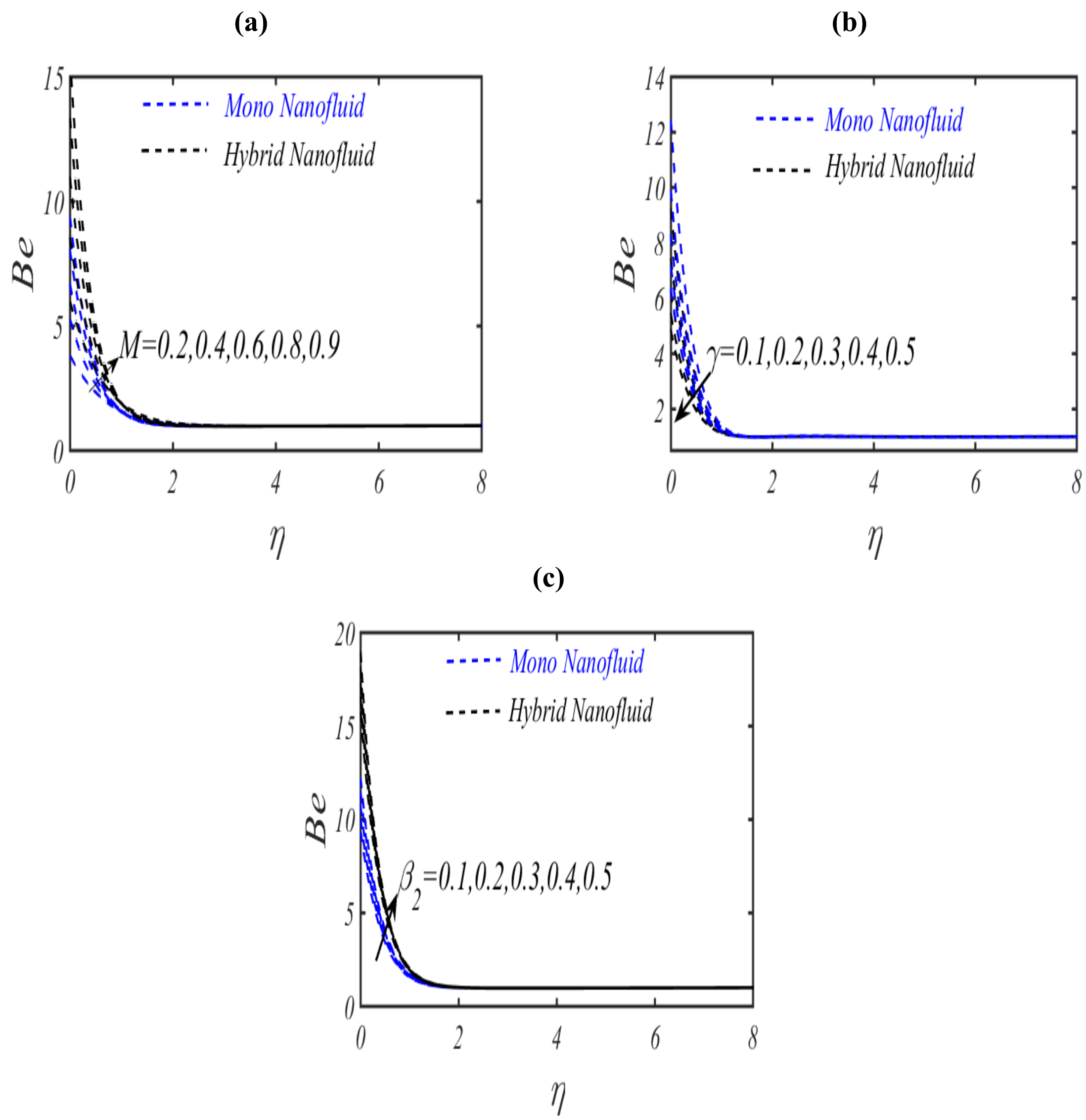

Fig. 6(a-c): Variation of Bejan number versus (a) M (b) γ (c) β_2.

Table 4: Numerical Simulations of local skin friction coefficient $Re_x^{\frac{-1}{2}}\ C\ f_x$ for various parameters

β_1	β_2	M	$(gold/Water)$	$(Gold - Copper/Water)$
0.2	0.5	0.2	0.5269	0.7024
0.5			0.5688	3.9525
0.8			3.5565	3.5836
	0.3		4.2524	4.2942
	0.7		4.7790	4.8145
	0.8		5.2710	5.3019
		0.1	5.1083	5.1451
		0.2	4.8952	4.9321
		0.3	4.7790	4.8145

Table 5: Contrast of Nusselt number $\left(Re_x^{\frac{-1}{2}} N u_x\right)$ for different parameters.

R	Ec	Bi	Pr	λ	β_3	$(gold/Water)$	$(Gold-Copper/Water)$
0.2	0.1	0.3	0.7	0.5	0.3	2.1244	3.4748
0.4						2.1686	3.6062
0.6						2.2089	3.7314
0.3	0.2					0.5508	1.2114
	0.5					0.1110	0.2631
	0.8					0.0101	0.0930
		0.2				0.1535	0.1711
		0.6				0.1560	0.1728
		0.8				0.1573	0.1738
			0.2			0.1489	0.1662
			0.6			0.1573	0.1738
			0.8			0.1426	0.1828
				0.4		0.2254	0.2895
				0.8		0.5903	0.7615
				1.2		0.6783	0.8753
					1.6	0.5408	0.6719
					2.5	0.7322	0.9751
					3.0	0.7565	1.0355

Table 6: Showcase the numerical outcomes of Sherwood number $\left(Re_x^{\frac{-1}{2}} S h_x\right)$ with various fluid parameters.

Sc	β	δ_c	$(gold/Water)$	$(Gold-Copper/Water)$
2.5	0.05	0.02	1.4632	1.4627
3			1.5194	1.5189
3.5			1.6768	1.5763
	0.01		1.2585	1.2583
	0.02		1.3782	1.3778
	0.03		1.4194	1.4189
		0.02	0.7835	0.7832
		0.03	1.1343	1.1339
		0.04	1.4194	1.4189

6. Conclusions

- The velocity profile declines due to relaxation number while increasing features are observed by varying retardation number.
- The heat transfer enhances due to Eckert number and heat source parameter.
- Change in retardation number enhances the temperature profile.
- The concentration profile reduces due to chemical reaction parameter and Schmidt number.
- The skin friction coefficient profile variation against retardation number enhances by varying Hartmann number.
- The Nusselt number increases with the Biot number.
- The entropy generation increases due to Hartmann number and Eckert number.
- The Bejan number gets enhance by varying the Hartmann number.

- Theoretical flow assumptions with ideal constraints were followed to model the problem. There may be discrepancies between the theoretical and experimental results.

- Future studies could recommend the modification in proposed model by performing the simulations through machine learning algorithms (Abbasi et al. (2025)).

Nomenclature

Nomenclature
Velocity components $(ms^{-1})[u, v]$
Viscosity $(kgm^{-1}s^{-1})[u]$
Density $(kgm^{-3})[\rho]$
Heat transfer coefficient$[h_f]$
Thermal radiation parameter $[R]$
Coefficient of skin friction $[C_f]$
Local Reynolds number$[Re_x\quad]$
Volume fraction $[\phi_1, \phi_2]$
Surface temperature $(K)[T_w]$
Temperature $(K)[T]$
Biot number$[Bi]$
Bejan number $[Be]$
Magnetic field strength $[B_0]$
Thermal conductivity$(W/mK)[k]$
Specific heat capacity$(J/kg)K[C_p]$
Radiative heat flux $[q_r]$
Stretching ratio parameter$[a]$
Maxwell relaxation time parameter $[\beta_1]$
Nusselt number $[Nu_x]$
Magnetic parameter $[M]$
Coordinates $(m)[x, y]$
Ambient temperature$(K)[T_\infty]$
Dimensionless temperature$(K)[\theta]$
Temperature gradient $[\gamma]$

References

Aamir, M., et al. (2025). Analysis for 3D thermal conducting micropolar nanofluid via artificial neural network." *The European Physical Journal Plus* 140, no. 2: 100.

Abbas, A., et al. (2022). MHD Williamson nanofluid fluid flow and heat transfer past a non-linear stretching sheet implanted in a porous medium: effects of heat generation and viscous dissipation." *Processes* 10, no. 6 (2022): 1221.

Abbasi, A. Z., et al. (2025). Modelling and prediction of 3D carreau fluid behaviour using machine learning for Cattaneo Christov Double diffusion with variable conductivity." *Case Studies in Thermal Engineering* 72: 106302.

Ahmad, M., et al. (2025). Buoyancy-driven bidirectional forced convection in chemically reactive Oldroyd-B nanofluid: incorporating the Cattaneo–Christov model with an external heat source for improved analysis." *Particulate Science and Technology* 43, no. 3: 369-381.

Ahmed, F., et al. (2024) Numerical modeling of a MHD non-linear radiative Maxwell nano fluid with activation energy." *Heliyon* 10, no. 2.

Akbar, A., A., et al. (2024). Heat transfer analysis of Carreau–Yasuda nanofluid flow with variable thermal conductivity and quadratic convection." *Journal of Computational Design and Engineering* 11, no. 1: 99-109.

Algehyne, E., A., et al. (2024). A numerical exploration of the comparative analysis on water and kerosene oil-based Cu–CuO/hybrid nanofluid flows over a convectively heated surface." *Scientific Reports* 14, no. 1: 2540.

Ali, N., et al. (2021). Carbon-based nanofluids and their advances towards heat transfer applications—a review." *Nanomaterials* 11, no. 6: 1628.

Asghar, A., et al. (2023). Magnetized mixed convection hybrid nanofluid with effect of heat generation/absorption and velocity slip condition." *Heliyon* 9, no. 2. e13189.

Assad, M., E., H., et al. (2021) Heat exchangers and nanofluids." In *Design and performance optimization of renewable energy systems*, pp. 33-42.

Aziz, S., et al. (2025) Hybrid nanofluid heat transfer optimization for energy storage applications." *International Communications in Heat and Mass Transfer* 169: 109904.

Bani-Fwaz, M., Z., et al. (2024). Computational investigation of thermal process in radiated nanofluid modulation influenced by nanoparticles (Al2O3) and molecular (H2O) diameters." *Journal of Computational Design and Engineering* 11, no. 2 (2024): 22-36.

Bhatti, M., M., et al. (2024). Numerical simulation for MHD Oldroyd-B fluid flow with melting and slip effect." *Scientific reports* 14, no. 1: 10591.

Eid, M., R., et al. (2022). Thermal conductivity variation and heat generation effects on magneto-hybrid nanofluid flow in a porous medium with slip condition." *Waves in random and complex media* 32, no. 3: 1103-1127.

Esfe, M., H., et al. (2022). Investigating the rheological behavior of a hybrid nanofluid (HNF) to present to the industry." *Heliyon* 8, no. 12.

Gope, R., et al. (2023). Hydro-thermo-fluidic aspects of Oldroyd B fluid with hybrid nanostructure subject to low and moderate Prandtl numbers." *Multidiscipline Modeling in Materials and Structures* 19, no. 2: 292-310.

Khan, S., U., et al. (2025). Machine learning-based thermal performances of hybrid nanofluid (Au–Ag/blood) with nonlinear radiative features for stretched surface flow." *Pramana* 99, no. 4: 167.

Khoramian, R., et al. (2022). The development of novel nanofluid for enhanced oil recovery application." *Fuel* 311 (2022): 122558.

Kumar, P., et al. (2021). Recent developments in preparation of nanofluid for heat transfer enhancement in heat exchangers: A review." *Materials Today: Proceedings* 44 (2021): 2356-2361.

Liu, L., et al. (2024). Construction of the absorbing boundary condition for the flow of Oldroyd-B fluid over a semi-infinite plate with magnetic effect." *Physics of Fluids* 36, no. 4.

Mebarek-Oudina, F., et al. (2024). Hybrid-nanofluid magneto-convective flow and porous media contribution to entropy generation." *International Journal of Numerical Methods for Heat & Fluid Flow* 34, no. 2: 809-836.

Munir, S., et al. (2025). Numerical analysis of entropy generation in the stagnation point flow of Oldroyd-B nanofluid. *Waves in Random and Complex Media* 35, no. 1: 465-481.

Nabwey, H., A., et al. (2022). A comprehensive review of nanofluid heat transfer in porous media." *Nanomaterials* 13, no. 5: 937.

Pavía, M., et al. (2021). A critical review on thermal conductivity enhancement of graphene-based nanofluids." *Advances in Colloid and Interface Science* 294: 102452.

Razzaq, R., et al. (2025). Artificial neural network modeling of heat transfer in bioconvective Oldroyd-B nanofluids with nonlinear radiation and activation energy." *Journal of Thermal Analysis and Calorimetry* (2025): 1-24.

Rehman, A., et al. (2024). Viscous dissipation effects on time-dependent MHD Casson nanofluid over stretching surface: A hybrid nanofluid study." *Journal of Molecular Liquids* 408: 125370.

Shah, Z., et al. (2023). Computational analysis of radiative engine oil-based Prandtl–Eyring hybrid nanofluid flow with variable heat transfer using the Cattaneo–Christov heat flux model." *RSC advances* 13, no. 6: 3552-3560.

Sharma, et al. (2022). Recent advances in machine learning research for nanofluid-based heat transfer in renewable energy system." *Energy & Fuels* 36, no. 13 (2022): 6626-6658.

Shoaib, M., et al. (2023). Stochastic numerical computing for hydro-magnetic flow of Carreau-nanofluid model." *Waves in Random and Complex Media*: 1-20.

Sohail, M., et al. (2025). Bio-convective boundary layer flow of Maxwell nanofluid via optimal homotopic procedure with radiation and Darcy-Forchheimer impacts over a stretched sheet." *International Journal of Ambient Energy* 46, no. 1 (2025): 2462583.

Wang, J., et al. (2023). "A review on nanofluid stability: preparation and application." *Renewable and Sustainable Energy Reviews* 188: 113854.